doi:10.1006/jmbi.2000.4203 available online at http://www.idealibrary.com on IDEAL® *J. Mol. Biol.* (2001) **305**, 905–915

JMB

The Crystal Structure of a Liganded Trehalose/Maltose-binding Protein from the Hyperthermophilic Archaeon *Thermococcus litoralis* at 1.85 Å

Joachim Diez, Kay Diederichs, Gerhard Greller, Reinhold Horlacher Winfried Boos and Wolfram Welte*

Department of Biology
University of Konstanz
78457 Konstanz, Germany

**Corresponding author*

We report the crystallization and structure determination at 1.85 Å of the extracellular, membrane-anchored trehalose/maltose-binding protein (TMBP) in complex with its substrate trehalose. TMBP is the substrate recognition site of the high-affinity trehalose/maltose ABC transporter of the hyperthermophilic Archaeon *Thermococcus litoralis*. *In vivo*, this protein is anchored to the membrane, presumably *via* an N-terminal cysteine lipid modification. The crystallized protein was N-terminally truncated, resulting in a soluble protein exhibiting the same binding characteristics as the wild-type protein. The protein shows the characteristic features of a transport-related, substrate-binding protein and is structurally related to the maltose-binding protein (MBP) of *Escherichia coli*. It consists of two similar lobes, each formed by a parallel β-sheet flanked by α-helices on both sides. Both are connected by a hinge region consisting of two antiparallel β-strands and an α-helix. As in MBP, the substrate is bound in the cleft between the lobes by hydrogen bonds and hydrophobic interactions. However, compared to maltose binding in MBP, direct hydrogen bonding between the substrate and the protein prevails while apolar contacts are reduced. To elucidate factors contributing to thermostability, we compared TMBP with its mesophilic counterpart MBP and found differences known from similar investigations. Specifically, we find helices that are longer than their structurally equivalent counterparts, and fewer internal cavities.

Keywords: maltose/trehalose transport; ABC transporter; thermostability; maltose-binding protein; trehalose-binding site

Introduction

High-affinity binding protein-dependent ABC transporters were originally discovered in Gram-negative bacteria. They consist of a high-affinity periplasmic substrate-binding protein as the major substrate recognition site, two hydrophobic membrane proteins spanning the cytoplasmic membrane and forming the translocation pore, and two additional cytoplasmic subunits, peripherally associated with the membrane proteins. By ATP hydrolysis, the latter two subunits provide the energy for the accumulation of substrate across the inner membrane against the concentration gradient.[1,2] Recently, it has been recognized that binding protein-dependent ABC transporters are present in Gram-positive bacteria.[3] In these cases, the soluble periplasmic binding proteins are anchored to the membrane by an N-terminal lipid modification. It consists of a diglyceride connected to the N-terminal cysteine residue *via* a thioether bond.[4] Binding protein-dependent ABC transporters have been found in thermophilic bacteria[5,6] and archaea,[7] and their binding proteins have been isolated and characterized.[8–10]

The crystal structures of several periplasmic substrate-binding proteins reveal a common blueprint. These proteins are composed of two separate but similarly folded globular domains or

Abbreviations used: MBP, maltose binding protein; TMBP, trehalose/maltose binding protein; P.f., *Pyrococcus furiosus*; BPD, bacterial binding protein-dependent.

E-mail address of the corresponding author: wolfram.welte@uni-konstanz.de

0022-2836/01/040905–11 $35.00/0

lobes, the N-terminal and the C-terminal lobe.[11] Both are connected by a hinge region made of two or three short polypeptide segments that are far apart in the polypeptide chain. Although the two lobes are formed by several non-contiguous polypeptide segments, they possess similar tertiary structure. They are composed of a central β-pleeted sheet of six or seven mostly parallel strands with two or three α-helices on each side forming a cleft between them. The structure analysis of unliganded and liganded members of this family has revealed a hinge movement of the two lobes, which thereby embrace the bound substrate and sequester it from bulk solvent. The maltose-binding protein (MBP) of *Echerichia coli* in particular has been subject to intensive structural analysis[12–20] as well as to kinetic analysis relevant to the substrate-induced conformational change.[21,22] Hydrogen bonds between the sugar and the protein as well as stacking of hydrophobic patches of the pyranose rings onto aromatic side-chains contribute to the high affinity of binding, which typically is in the μM range.

We present here a structure analysis of the trehalose/maltose-binding protein (TMBP) belonging to the first characterized archaeal binding protein-dependent ABC transporter from the hyperthermophilic *Thermococcus litoralis*. The genes for the transport system (including *malE* encoding TMBP) are contained on a 16 kb DNA fragment that can be found in nearly identical sequences flanked with insertion elements in *Pyrococcus furiosus*, demonstrating lateral gene transfer between these two organisms. In addition to this acquired trehalose/maltose ABC transporter, *P. furiosus* contains a second ABC transporter that recognizes maltose and maltotriose but not trehalose. This latter system is not present in *T. litoralis*.[23] The binding proteins of these two *P. furiosus* transporters can be aligned with 27% identical residues. The structure determination of the maltose/maltotriose-binding protein from *P. furiosus* is presented in the accompanying paper.[24]

TMBP in its natural host is membrane-attached but can be solubilized by detergents. The nature of its membrane attachment is not clear at present. Based on the presence of an N-terminal signal sequence typical for cysteine lipid modification in Gram-positive bacteria,[3,4] we proposed[8] that the protein is anchored to the membrane *via* lipids. Yet, in a recent study of a glucose transporter of the hyperthermophilic *Solfolobus solfataricus* with sequence similarity to TMBP, it was shown that the cognate binding protein was attached to the membrane by an N-terminal anchor helix,[25] which in the TMBP sequence we had interpreted as a signal sequence. We believe an anchor helix in TMBP to be unlikely, since a cysteine residue is surrounded by amino acids typical for secretion cleavage and lipid modification. For the structural analysis reported here, we truncated the protein at the N terminus, replacing its natural signal sequence with the *E. coli* MBP signal sequence, and expressed the protein in *E. coli*. Surprisingly, only a minor fraction of TMBP was secreted, while active TMBP accumulated in the cytoplasm. The N terminus of TMBP was uniformly cleaved by endogenous proteases six residues N-terminally from the expected cleavage site of the *E. coli* signal sequence. The resulting soluble protein exhibits the same binding characteristics as the wild-type protein.

Results and Discussion

Tertiary structure of TMBP

TMBP and MBP share a common fold with other sugar-binding proteins.[12,13,26–31] These proteins consist of two globular domains (lobes), with a similar tertiary structure consisting of a central pleated β-sheet, which is flanked by α-helices (Figure 1). The hinge is formed by the loops between β4 and β5, between β11 and β12 and between α14 and α15. The groove between the two lobes contains the sugar-binding site. We compared the structure of TMBP with known structures of other sugar-binding proteins (arabinose-binding protein,[27] ribose-binding protein,[29] allose-binding protein,[31] glucose/galactose-binding protein,[28] and maltose-binding protein[20].) The highest similarity of the overall structure is found between TMBP and MBP: 278 C^{α} atoms of both can be superimposed with a root-mean-square

Figure 1. Ribbon model of TMBP with bound trehalose (shown as a ball and stick model). The N-terminal and C-terminal lobes are coloured yellow and blue, respectively. The bound trehalose is shown as a bond model and coloured black; α-helices and β-strands are labelled according to Figure 2(b).

Table 1. Amino acid composition of TMBP and MBP (%)

	Charged	Polar	Apolar	Val	Leu	Ile	Tyr	Ala	Gly/Pro/Phe/Asn/Gln
MBP	26.2	28.6	45.2	5.4	8.1	6.2	4.1	11.9	29.8
TMBP	25.9	30.7	43.4	8.8	8.3	3.9	5.6	7.3	30.0

deviation (rmsd) of 1.75 Å (cutoff at 3.0 Å). For this reason, and as both bind maltose with high affinity, we compared the structures of TMBP complexed with trehalose and of MBP complexed with maltose (Figure 2(a)). The structural alignment (Figure 2(b)) of the two proteins shows that the sequence of helices, turns and β-structures in both proteins is identical despite the low amino acid sequence identity (28 %).

Evdokimov *et al.*[24] describe the structure of a maltose-binding protein from the hyperthermophilic archaeon *P. furiosus*, which is also structurally and functionally related with MBP (P.f.MBP). This protein can be superimposed with TMBP with a rmsd of 1.66 Å (cutoff at 3.0 Å).

Thermostability

In most studies that compared mesophilic and thermophilic proteins, only subtle differences were detected.[32–36]

One factor for thermostability identified in most studies is the difference in amino acid composition between mesophilic and thermophilic homologs. The most stable amino acids in solution are valine and leucine, followed by isoleucine and tyrosine.[35,37–39] The most unstable amino acids in solution are alanine, glycine, proline, asparagine, glutamine and phenylalanine. However, the differences in amino acid composition between MBP and TMBP (Table 1) appear rather insignificant. When the percentages of charged, polar and hydrophobic amino acids are compared, a slight preference for more hydrophilic residues is observed in TMBP. A slight preference for valine and tyrosine is seen in TMBP, while Ala and Ile are reduced.

When the structures of TMBP and MBP are superimposed (Figure 2), an elongation of nearly all α-helices in TMBP becomes apparent, and an additional helix (α6, residues 131-136) is found. Apparently, the elongation of α-helices has a thermostabilizing effect on the structure[40,41] by the increased number of backbone hydrogen bonds.

The solvent-accessible surface area and the specific volume of both proteins are rather similar (see Table 2). This is different from other thermophilic proteins, which were shown to have a more compact structure than their mesophilic equivalents.

Thermophilic proteins tend to possess fewer intramolecular cavities. When the total volume of all cavities in the two proteins is compared (Table 2), a major difference is seen. While MBP has 11 cavities with an overall volume of 602.9 Å^3, TMBP has only five cavities with an overall volume of 121.1 Å^3. This makes sense, as thermostability is furthered by increasing van der Waals energy, i.e. by avoiding empty cavities.

The sugar-binding site

In the cleft between the N and C-terminal lobes, electron density corresponding to α,α-trehalose was found as shown in Figure 3. The binding of the ligand is established by interactions known from many sugar-binding proteins.[11]

The disaccharide is held in position by hydrogen bonds and van der Waals contacts. All the hydroxyl groups and even the glycosidic oxygen atom as well as the ring oxygen atom of one glucosyl residue (Glc1) participate in hydrogen bonding. In total, 21 hydrogen bonds are formed with the protein and three hydrogen bonds are formed with

Table 2. Solvent-accesible surfaces, volumes and cavities in TMBP and MBP

	TMBP	MBP
Solvent-accessible surface (Å^2)	13675.3	12627.0
Surface of apolar side-chains (Å^2)	7494.1 (54.8 %)	6944.9 (55.0 %)
Surface of polar side-chains (Å^2)	4430.8 (32.4 %)	4015.4 (31.8 %)
Surface of main-chain (Å^2)	1750.4 (12.8 %)	1666.7 (13.2 %)
Molecular volume of the protein (Å^3)	54,455.1	49,210.3
Volume of cavities (Å^3)	112.1	602.9
Volume of the protein with excluded volume of the cavities (Å^3)	54,342.0	48,607.4
Compactness[a]	16.6	17.0

[a] Compactness = molecular volume (with excluded cavity volume) of the protein/total number of structured atoms in the-oligomer.

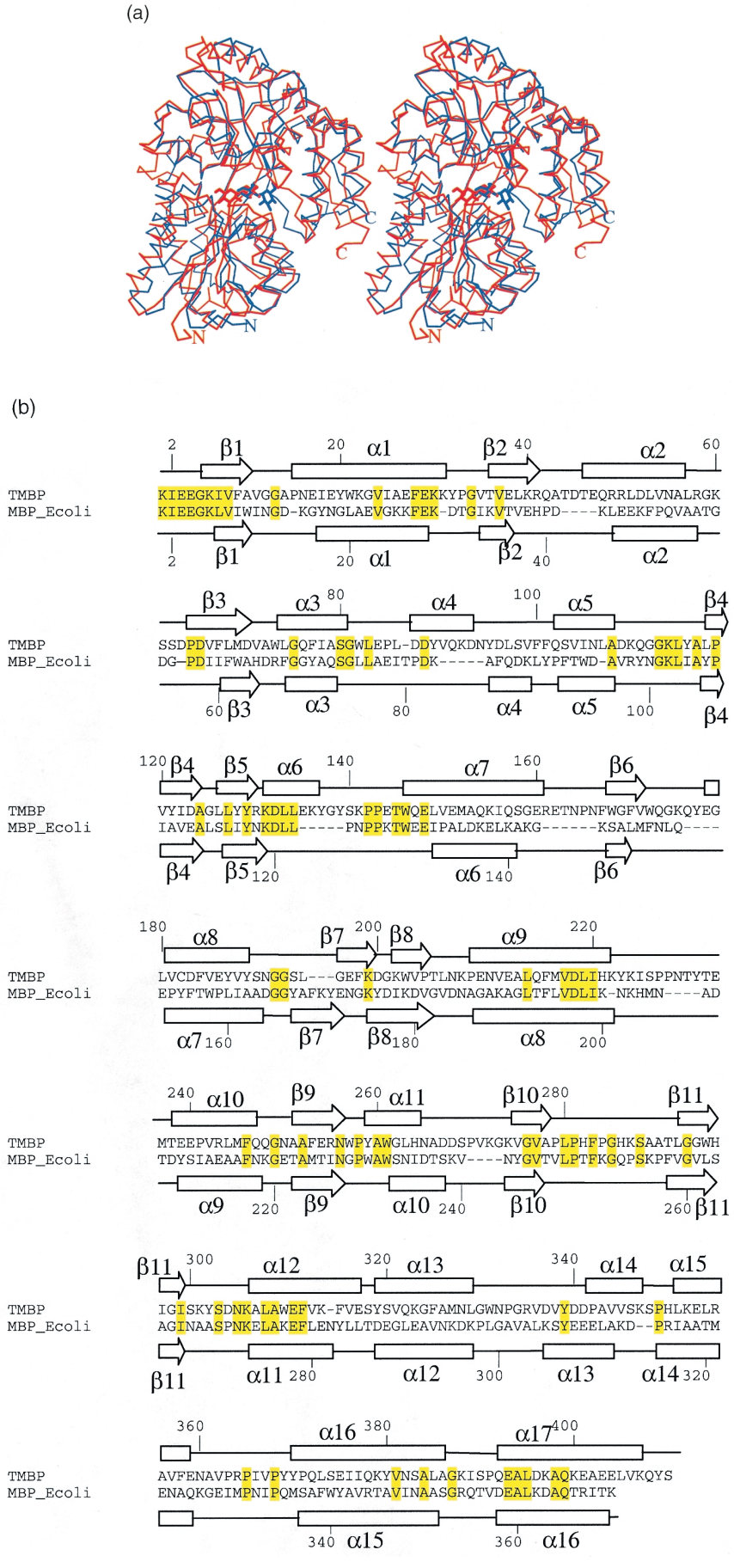

Figure 2 (*legend opposite*)

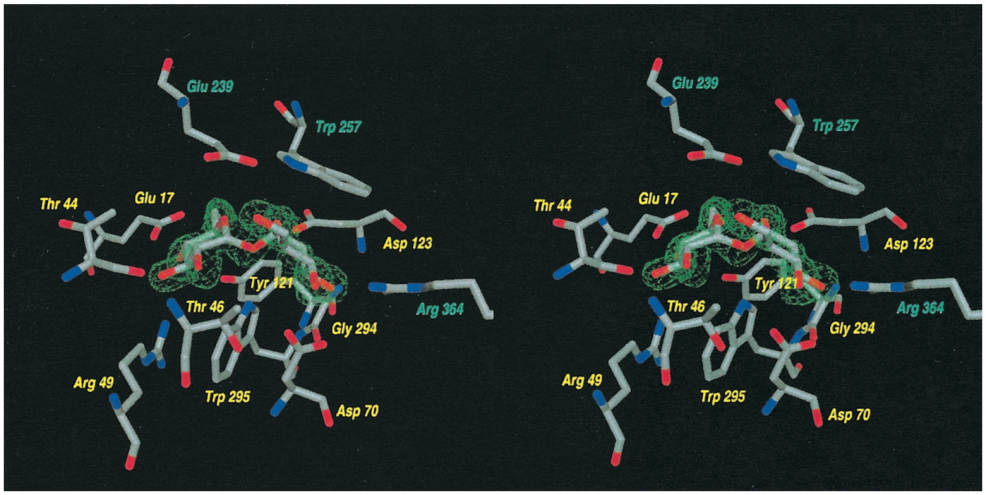

Figure 3. Stereo representation of a $|3F_o - 2F_c|$ electron density map of TMBP at 2.4 σ around the bound α,α-trehalose moiety. Carbon atoms are coloured grey, nitrogen atoms are coloured blue and oxygen atoms are coloured red. The map is coloured green.

two water molecules (Table 3). These are unequally distributed over the two identical glucosyl residues, with Glc1 forming slightly more hydrogen bonds (14) than Glc2 (ten). The TMBP complex with trehalose is thus established by a larger number of hydrogen bonds than the MBP complex with maltose[20] (11 with the protein and three with water). Thus, the binding site of TMBP appears to be more polar.

When the structures of the two proteins are superimposed (Figure 2(a)), Glc1 of trehalose bound to TMBP fits exactly to Glc1 of maltose (the reducing glucosyl residue) bound to MBP. Glc2 of the trehalose moiety in TMBP is located differently in comparison to the Glc2 of maltose in MBP (the non-reducing glucosyl residue). Whereas Glc2 of maltose is directed towards the core of MBP, in TMBP Glc2 of trehalose is located closer to the surface of the protein (Figure 2(a)) and forms van der Waals contacts with Trp295 (see Table 3). Thus, only the Glc1 residues in both liganded proteins are structurally equivalent and can be compared for their amino acid surroundings. Although they hold equivalent positions, their binding mode is different, showing the same general shift to hydrogen bonding in TMBP (14 bonds) as compared to MBP (five bonds) as mentioned above. Even though the binding residues are not conserved, some structurally equivalent residues are apparent. Glu111 in MBP is conservatively exchanged to Asp123 in TMBP. Tyr155 in MBP, which provides van der Waals contacts, is equivalent to Trp257 in TMBP. As a second feature, Trp257 in MBP forms a hydrogen bond with O5 from Glc1. The two other hydrogen bond donors of MBP, residues Asp14 and Lys15, correspond to Asp70 and Arg364 of TMBP, although they differ in side-chain conformation.

Temperature-dependence of substrate association and dissociation

Transport of trehalose in intact cells of *T. litoralis* is temperature-dependent and maximal only at 80 °C. Similarly, when trehalose binding by TMBP is tested at subsaturating concentrations by the ammonium sulfate precipitation technique, the amount of trehalose bound at constant TMBP concentration peaked at 80 °C. At that temperature, a K_d of 0.16 μM was determined by exit dialysis.[8] To study association and dissociation of substrate more closely, we first removed any bound ligand by dialyzing the protein against 6 M guanidinium hydrochloride followed by dialysis against 50 mM sodium phosphate buffer (pH 7.0), which completely renatured the protein (as tested by ammonium sulfate binding assays at 80 °C). The following assay is based on the phenomenon that binding of maltose to TMBP increases fluorescence whereas binding of trehalose reduces fluorescence.[8] First, binding of maltose at saturating concentrations (5 μM) was followed by observing the fluorescence

Figure 2. (a) Superposition (stereo) of the C^{α} traces of TMBP with bound trehalose (coloured red) and MBP from *E. coli* with bound maltose (coloured blue). (b) Structural alignment of TMBP and MBP. The numbering of the residues is as explained in Materials and Methods. α-Helices and β-strands are indicated by boxes and arrows, respectively, and numbered consecutively. Conserved residues are underlined in yellow.

Table 3. The binding site of TMBP

Polar contacts (<3.5 Å)						Van der Waals contacts (<4 Å)			
Sugar atom		Protein/water atom		Location	Distance (Å)	Sugar subunit	Location	No. of contacts	Residues
Glc1	O1	NE1	Trp295	N-domain	3.24	Glc1	C-domain	5	Trp257
	O2	N	Gly294	N-domain	2.91		C-domain	1	Gly179
	O2	NE1	Trp295	N-domain	3.50		C-domain	1	Glu178
	O2	OD2	Asp123	N-domain	2.57				
	O3	N	Gly294	N-domain	3.10				
	O3	OD1	Asp70	N-domain	2.78				
	O3	NH2	Arg364	C-domain	3.03				
	O4	OD2	Asp70	N-domain	2.60				
	O4	NH1	Arg364	C-domain	2.81				
	O4	NH2	Arg364	C-domain	3.42				
	O5	NE1	Trp257	C-domain	3.10				
	O5	OE2	Glu239	C-domain	3.21				
	O6	OE2	Glu239	C-domain	2.89				
	O6		Water		2.81				
Glc 2	O2	O	Thr44	N-domain	2.72	Glc2	N-domain	1	Gly13
	O2	N	Thr46	N-domain	3.51		C-domain	2	Tyr259
	O3	NH1	Arg49	N-domain	2.81		N-domain	2	Trp295
	O3	O	Thr44	N-domain	2.75		C-domain	1	Gly13
	O4	OE1	Glu17	N-domain	2.62				
	O4	OH	Tyr121	N-domain	3.24				
	O6	OE2	Glu17	N-domain	2.76				
	O6	OH	Tyr121	N-domain	3.00				
	O2		Water		2.78				
	O6		Water		2.98				

Residues that are within hydrogen-bonding distance (<3.5 Å) and van der Waals contact distance (<4 Å) of the trehalose ligand.

increase at 340 nm. The substrate-free TMBP showed an immediate increase in fluorescence at all temperatures tested (15-80 °C) that was completed within the time of data sampling (less than two seconds). This indicates that binding of substrates to the empty and supposedly open form of TMBP is fast in the whole temperature range. Thus, the movement of the two lobes (as measured by fluorescence increase) to enclose the substrate maltose is not compromized at room temperature. In contrast, when subsequently trehalose was added at competing concentration (100 μM) to exchange the TMBP-bound maltose, the subsequent kinetic of reduction of fluorescence decrease, characteristic for trehalose binding, is found to be strongly temperature-dependent. The half-time required to reach the quenched value indicative for the trehalose-bound form of TMBP increases with falling temperature. The following half-times (in minutes) were observed: less than 0.05 (82 °C), 0.08 (67 °C), 0.1 (59 °C), 0.25 (48 °C), 0.5 (39 °C), 0.7 (31 °C), 0.8 (22 °C). This demonstrates that it is the opening of the two lobes of TMBP that is slowed at ambient temperatures when compared to MBP of *E. coli*.

The different changes in fluorescence with maltose (increasing) and trehalose (decreasing) indicate that maltose is bound to TMBP and to MBP in a similar manner, i.e. such that the non-reducing glucose moiety (Glc2) is located remote from Trp295 (Figures 2(a) and 3). This placement can explain both the quenching of the fluorescence in TMBP by the van der Waals contact of Glc2 of trehalose with Trp295 and the absence of quenching by maltose.

Putative restraints guiding the evolution of periplasmic binding proteins in hyperthermophilic archaea

The organization of the *T. litoralis* trehalose/maltose transport operon.[8,42] is very similar to that of *E. coli* and other bacterial binding protein-dependent (BPD) ABC transport systems.[1,43] In *E. coli*, the maltose transport system is in fact a maltodextrin transport system optimized for the utilization of maltose as well as of short maltodextrins. This can be deduced from the function of the outer membrane λ-receptor as a diffusion pore for short maltodextrins,[30] the binding specificity of MBP, as well as from the characteristics of the maltodextrin-degrading enzymes.[43] In contrast, the *T. litoralis* uptake system accepts only trehalose and maltose[7] (with a K_m of 20 nM), whereas the K_d of the binding protein for both substrates is 0.16 μM.[8] Maltotriose is accepted less well and longer maltodextrins are not accepted.

In order to achieve binding affinity, the energy of interaction must overcome the free energy contribution due to the entropy gain upon dissociation. Shorter-chain oligosaccharides therefore need to be bound at higher energies of interaction per glucose residue than longer oligosaccharides.

There must be an upper limit to affinity determined by the mechanism of the ATP-driven uptake of the transporter and a lower limit set by the efficiency of the uptake process. The interaction energy can be enthalpic by hydrogen bonds and van der Waals contacts as well as hydrophobic by sequestering hydrophobic faces of pyranose rings from water upon stacking onto aromatic side-chains. The latter entropic contribution increases with temperature.

In the maltose-binding proteins of *T. maritima* and of *E. coli*, the binding affinity *in vitro* increases with temperature. This is indicative for a strong contribution by hydrophobic energies in binding of maltose and maltotriose.

The maltose-binding protein of *P. furiosus* binds the same sugars in the same temperature range as the *T. maritima* protein but with different thermodynamic parameters, as described in the accompanying paper.[24] *P. furiosus* surprisingly has a second homologous transporter with a binding protein identical with TMBP. TMBP binds the two disaccharides trehalose and maltose. The acquisition of this system by *P. furiosus* was the result of a recent lateral gene transfer, most likely from *T. litoralis* to *P. furiosus*.[23]

Hydrophobic energies of interaction may be disadvantageous for TMBP because a suitable geometry of aromatic residues fitting to two disaccharides with different angles between their two glucose moieties may be difficult to establish. A large number of hydrogen bonds, as found between trehalose and TMBP, may be the best solution to achieve high affinity for both disaccharides. When more residues are involved in hydrogen bonding, they can form two sets of polar residues, each one binding one of the two sugars. On the other hand, the maltose/maltodextrin-binding proteins bind ribbon-shaped strings of 1,4-linked glucose residues with one surface slightly different in polarity from the other. In this case, binding sites with a suitable arrangement of aromatic residues for extensive hydrophobic stacking may be built more easily and may be advantageous at high temperatures.

Materials and Methods

Expression and purification of TMBP

E. coli SF120[44] was transformed with plasmid pRHo1000.[8] The expressed protein contains residues 46 to 450 of the derived amino acid sequence fused to 11 N-terminal residues of *E. coli* MBP. To allow comparison with the latter, we have in the following numbered the residues of the fusion protein beginning with the N terminus of the processed MBP. The TMBP sequence thus starts in our scheme (Figure 2(b)) at Lys6, which corresponds to Lys46 in the derived amino acid sequence of TMBP. Cells were cultivated at 30 °C in 10 l of NZA-Medium (10 g of NZ-Amine A, 5 g of yeast extract and 7.5 g of NaCl per litre) containing 250 mg/ml ampicillin. After an absorbance of 0.5 was reached, expression of the *malE* gene was induced by adding IPTG to a final concentration of 100 μM. The cells were incubated for eight hours and afterwards harvested by centrifugation (ten minutes at 10,000 *g*). The cells were then ruptured in a French press cell at 10,000 psi (1 psi ≈ 6.9 kPa) and centrifuged for 20 minutes at 75,000 *g*. The supernatant was treated with DNase I and RNase I and stirred for 20 minutes at room temperature followed by heating the solution for 20 minutes at 80 °C. After centrifugation for ten minutes at 75,000 *g*, the clarified protein solution was dialyzed against 30 mM Tris-HCl (pH 7.5). The protein was purified in two steps using fast protein liquid chromatography. The first step consisted of an anion-exchange column (Q-Sepharose, fast flow) with a linear salt gradient of 0 to 100 mM NaCl. TMBP eluted at 35 mM NaCl. After dialyzing the eluted protein against 50 mM histidine (pH 6.2) the solution was applied to a chromatofocussing column (PBE 94) in the same buffer. A linear pH-gradient from pH 6.2 to pH 4.5 was used to elute the protein. Two peaks (at pH 5.5 and at pH 5.0) contained TMBP. Only the TMBP eluting at a pH of 5.0 crystallized. Routinely, we obtained 5 mg of homogeneous TMBP of the pH 5.0 fraction from 10 l of culture medium.

Fluorescence measurements

Soluble TMBP was used at 20 mg/ml. Fluorescence was measured in a Perkin-Elmer 650-40 Fluorescence Spectrophotometer at an excitation wavelength of 280 nm and an emission wavelength of 344 nm. Fluorescence was monitored until the fluorescence drift came to a standstill. Addition of substrate into the stirred solution was done in 10 ml aditions of 100-fold concentrated solutions.

Crystallization and structure solution

Crystals were grown at 18 °C using the hanging drop vapor diffusion method with the aid of Hampton Research screening solutions. Successful crystallization required the TMBP solution to be incubated with 1 mM α,α-trehalose at 80 °C for ten minutes, and subsequent removal of unbound trehalose by dialysis against 10 mM Tris-HCl (pH 7.5) at room temperature.

The crystallization buffer contained 25 % (w/v) polyethylene glycol 4000, 200 mM ammonium sulfate and 100 mM sodium acetate (pH 4.6). Drops were prepared by mixing 5 μl of TMBP solution (6 mg/ml) with 5 μl of crystallization buffer. Crystals appeared after eight weeks. For data collection at 100 K the crystals were soaked for one minute in the crystallization buffer supplemented with 20 % glycerol. The crystals were rapidly frozen and stored in liquid nitrogen.

Heavy-atom derivatives were obtained by conventional soaking methods: 1 μl of each compound was added to the crystallization drop and the crystals were incubated for eight hours in the crystallization buffer containing the heavy-atom salt (1 mM K_2PtCl_4 and 1 mM $KHgI_4$). Data sets were measured using rotating anode and synchrotron X-ray sources at 100 K using Mar345 image plate detectors.

Native crystals diffracted to 2.35 Å on a rotating anode X-ray source. Data from a crystal soaked with K_2PtCl_4 were collected to 1.85 Å at a synchrotron X-ray source (BW7B, DESY/EMBL, Hamburg). A dataset from a crystal soaked with $KHgI_4$ was collected to 2.9 Å on a rotating anode X-ray source. Parameters of the data sets are summarized in Table 4.

Table 4. Statistics on data reduction and MIRAS phasing for TMBP data sets

	Native dataset $\lambda = 1.54$ Å	K_2PtCl_4 dataset $\lambda = 0.84390$ Å	K_2PtCl_4 dataset $\lambda = 1.54$ Å	$KHgI_4$ dataset $\lambda = 1.54$ Å
Resolution (Å)	20-2.35	20-1.85	20-2.9	20-3.0
No. of unique observations	17,825 (2960)	67,503 (4665)	17,781 (1697)	13,885 (4635)
Completeness (%)	98.8 (98.5)	97.7 (87.4)	99.2 (97.2)	77.5 (77.2)
R_{merged} (%)	8.6 (23.3)	8.0 (33.7)	17.3 (33.5)	15.0 (37.6)
Isomorphous phasing power		0.94 (0.69)	0.66 (0.53)	0.70 (0.63)
Anomalous phasing power		1.34 (0.72)	0.65 (0.34)	0.67 (0.30)

The values for the highest resolution shell are given in parentheses.

The data were processed using the XDS[45] program suite or the HKL[46] program suite. Scaling and merging of the integrated intensities was performed using XSCALE,[45] TRUNCATE[47] and CAD[47] programs. The crystals grow in space group $P2_12_12_1$ ($a = 59.24$ Å, $b = 81.53$ Å, $c = 86.46$ Å) with one molecule per asymmetric unit.

The structure was solved using MIRAS with the help of two heavy-atom derivatives (see Table 4). The heavy-atom sites were found using the program SOLVE.[48] Further refinement of the heavy-atom sites was performed using SHARP.[49] This led to a heavy-atom model containing three Pt and three Hg sites. In the Pt derivative, one major and two minor sites could be detected. Due to the high resolution of the Pt dataset we were able to include the Pt sites and three chloride ions of the major Pt site to further improve the phases.

The resulting electron density map was solvent flattened using the program SOLOMON[47,50] and was used for a six-dimensional real-space molecular replacement search, which was performed with a parallelized version[51] of the program ESSENS,[52] using a polyserine model of *E. coli* MBP as a template.

Maps ($3F_o - 2F_c$ and $F_o - F_c$) were calculated with the CNS[53] program suite. For phase calculation, initially the native dataset to 2.35 Å was utilized. For refinement, however, we used the 1.85 Å K_2PtCl_4 dataset and modelled the complex of the protein with the heavy-atom compound. Model building was perfomed using the program O.[54] Simultaneously, automatic model building was performed using the ARP/WARP[55] program suite and the calculated map was used as an additional template for model building. The calculated phases from SHARP were used for map calculation and as a refinement target until R_{free} dropped below 40 %.

The initial model refinement was done by manual model building, grouped *B*-factor refinement and energy minimization steps and, after R_{free} dropped below 36 %, refinement was performed using individual *B*-factor refinement, torsion angle dynamics by slow cooling the model after heating to 2000 K and energy minimization. The quality of the structure was analyzed using PROCHECK[56] and WHAT IF[57] (Table 5). The final model comprises four N-terminal residues of *E. coli* MBP followed by residues 46 to 450 of the unprocessed form of TMBP, one trehalose molecule, three platinum sites with, overall, five chlorine atoms and 296 water molecules: 12 further residues at the N terminus could not be modelled due to lack of density.

After completion of the refinement against the 1.85 Å derivative dataset, the resulting model was used for refinement against the 2.35 Å dataset (*R* 20.9 %, R_{free} 25.8 %). As no significant deviation between the final models was found, and the rms deviations are low (0.25 Å for backbone atoms), the analyses reported here were based on the better-defined model based on the higher-resolution data.

Table 5. Crystallographic refinement statistics of the TMBP structure

Protein atoms	3267
Ligand atoms	23
Heavy-atom compound atoms	8
Solvent atoms	289
Resolution range (Å)	20-1.85
R-factor (%)	19.8
R-free (%)	23.2
rms bond length deviations (Å)	0.007
rms bond angles deviations (deg.)	1.306
Ramachandran plot[a]	
Most favored regions (%)	90.8
Additional allowed regions (%)	8.9
Generously allowed regions (%)	0.3
Disallowed regions (%)	0.0
Average *B*-factor main-chain/side-chain/ water (Å^2)	21.0/23.2/32.7

[a] As defined by PROCHECK.[56]

Secondary and tertiary structure analysis

The secondary structures of TMBP and MBP were determined with the DSSP program suite.[58] Calculations of the surface area and their hydrophobicity/hydrophilicity were done with the help of the NACCESS program suite (S. J. Hubbard & J. M. Thornton, Department of Biochemistry and Molecular Biology, University College, London). Internal cavities were determined using GRASP[59] with a probe radius for water of 1.4 Å.

Protein Data Bank accession code

The coordinates of TMBP with bound trehalose were deposited at the RCSB Protein Data Bank under ID code 1EU8.

Acknowledgments

This work was supported by the Deutsche Forschungsgemeinschaft. X-ray data were collected at the EMBL BW7B beamline at the DORIS storage ring, DESY, Hamburg. The authors thank Paul Tucker for his help at

the EMBL beamline, Svenja Thurau, and Richard Wonka for crystallization experiments, and Renate Riek for fluorescence measurements.

References

1. Boos, W. & Lucht, J. M. (1996). Periplasmic binding protein-dependent ABC transporters. In Escherichia coli *and* Salmonella typhimurium; Cellular and Molecular Biology (Neidhardt, F. C., Curtiss, R., Ingraham, J. L., Lin, E. C. C., Low, K. B., Magasanik, B., Reznikoff, W. S., Riley, M., Schaechter, M. & Umbarger, H. E., eds), 2nd edit., vol. 1, pp. 1175-1209, American Society of Microbiology, Washington, DC.
2. Diederichs, K., Diez, J., Greller, G., Müller, C., Breed, J., Schnell, C., Vonrhein, C., Boos, W. & Welte, W. (2000). Crystal structure of MalK, the ATP-hydrolyzing subunit of the trehalose/maltose ABC transporter of the hyperthermophilic archaeon *Thermococcus litoralis*. *EMBO J.* **19**, 5951-5961.
3. Gilson, E., Alloing, G., Schmidt, T., Claverys, J. P., Dudler, R. & Hofnung, M. (1988). Evidence for high affinity binding-protein dependent transport systems in gram-positive bacteria and in Mycoplasma. *EMBO J.* **7**, 3971-3974.
4. Wu, H. C. (1996). Biosynthesis of lipoproteins. In Escherichia coli *and* Salmonella typhimurium; Cellular and Molecular Biology (Neidhardt, F. C., Curtiss, R., Ingraham, J. L., Lin, E. C. C., Low, K. B., Magasanik, B., Reznikoff, W. S., Riley, M., Schaechter, M. & Umbarger, H. E., eds), pp. 1005-1014, American Society of Microbiology, Washington, DC.
5. Herrmann, A., Schlösser, A., Schmid, R. & Schneider, E. (1996). Biochemical identification of a lipoprotein with maltose-binding activity in the thermoacidophilic Gram-positive bacterium *Alicyclobacillus acidocaldarius*. *Res. Microbial.* **147**, 733-737.
6. Sahm, K., Matuschek, M., Müller, H., Mitchell, W. J. & Bahl, H. (1996). Molecular analysis of the *amy* gene locus of *Thermoanaerobacterium thermosulfurigenes* EM1 encoding starch-degrading enzymes and a binding protein-dependent maltose transport system. *J. Bacterial.* **178**, 1039-1046.
7. Xavier, K. B., Martins, L. O., Peist, R., Kossmann, M., Boos, W. & Santos, H. (1996). High affinity maltose/trehalose transport system in the hyperthermophilic Archeon *Thermococcus lithoralis*. *J. Bacteriol.* **178**, 4773-4777.
8. Horlacher, R., Xavier, K. B., Santos, H., DiRuggiero, J., Kossmann, M. & Boos, W. (1998). Archaeal binding protein-dependent ABC transporter: molecular and biochemical analysis of the trehalose/maltose transport system of the hyperthermophilic archaeon *Thermococcus litoralis*. *J. Bacteriol.* **180**, 680-689.
9. Albers, S. V., Elferink, M. G. L., Charlebois, R. L., Sensen, W., Driessen, A. J. M. & Konings, W. N. (1999). Glucose transport in the extremely thermoacidophilic *Sulfolobus solfataricus* involves a high-affinity membrane-integrated binding protein. *J. Bacteriol.* **181**, 4285-4291.
10. Wassenberg, D., Liebl, W. & Jaenicke, R. (2000). Maltose-binding protein from the hyperthermophilic bacterium *Thermotoga maritima*: stability and binding properties. *J. Mol. Biol.* **295**, 279-288.
11. Quiocho, F. A. & Ledvina, P. S. (1996). Atomic structure and specificity of bacterial periplasmic receptors for active transport and chemotaxis: variation of common themes. *Mol. Microbiol.* **20**, 17-25.
12. Spurlino, J. C., Lu, G.-Y. & Quiocho, F. A. (1991). The 2.3-Å resolution structure of the maltose- or maltodextrin-binding protein, a primary receptor of bacterial active transport and chemotaxis. *J. Biol. Chem.* **266**, 5202-5219.
13. Spurlino, J. C., Rodseth, L. E. & Quiocho, F. A. (1992). Atomic interactions in protein-carbohydrate complexes - tryptophan residues in the periplasmic maltodextrin receptor for active transport and chemotaxis. *J. Mol. Biol.* **226**, 15-22.
14. Sharff, A. I., Rodseth, L. E., Spurlino, J. C. & Quiocho, F. A. (1992). Crystallographic evidence of a large ligand-induced hinge-twist motion between the two domains of the maltodextrin binding protein involved in active transport and chemotaxis. *Biochemistry,* **31**, 10657-10663.
15. Rodseth, L. E. & Quiocho, F. A. (1993). Crystallization of the maltodextrin-binding protein for active transport and chemotaxis in several different liganded and mutant forms. *J. Mol. Biol.* **230**, 675-678.
16. Sharff, A. J., Rodseth, L. E. & Quiocho, F. A. (1993). Refined 1.8-Å structure reveals the mode of binding of β-cyclodextrin to the maltodextrin binding protein. *Biochemistry,* **32**, 10553-10559.
17. Shilton, B. H., Shuman, H. A. & Mowbray, S. L. (1996). Crystal structures and solution conformations of a dominant-negative mutant of *Escherichia coli* maltose-binding protein. *J. Mol. Biol.* **264**, 364-376.
18. Shilton, B. H., Flocco, M. M., Nilsson, M. & Mowbray, S. L. (1996). Conformational changes of three periplasmic receptors for bacterial chemotaxis and transport: the maltose-, glucosel/galactose- and ribose-binding proteins. *J. Mol. Biol.* **264**, 350-363.
19. Hall, J. A., Gehring, K. & Nikaido, H. (1997). Two modes of ligand binding in maltose-binding protein of *Escherichia coli*. Correlation with the structure of ligands and the structure of binding protein. *J. Biol. Chem.* **272**, 17605-17609.
20. Quiocho, F. A., Spurlino, J. C. & Rodseth, L. E. (1997). Extensive features of tight oligosaccharide binding revealed in high-resolution structures of the maltodextrin transport/chemosensory receptor. *Structure,* **5**, 997-1015.
21. Thomson, J., Liu, Y., Sturtevant, J. M. & Quiocho, F. A. (1998). A thermodynamic study of the binding of linear and cyclic oligosaccharides to the maltodextrin-binding protein of *Escherichia coli*. *Biophys. Chem.* **70**, 101-108.
22. Döring, K., Surrey, T., Nollert, P. & Jähnig, F. (1999). Effects of ligand binding on the internal dynamics of maltose-binding protein. *Eur. J. Biochem.* **266**, 477-483.
23. DiRuggiero, J., Dunn, D., Maeder, D. L., Holley-Shank, R., Chatard, J., Horlacher, R., Robb, F. T. & Boos, W. (2000). Evidence of lateral gene transfer among hyperthermophilic archaea. *Mol. Microbiol.* **38**, 684-693.
24. Evdokimov, A. G., Anderson, D. E., Rautzahn, K. M. & Waugh, D. S. (2000). Structural basis for oligosaccharide recognition by *Pyrococcus furiosus* maltodextrin-binding protein. *J. Mol. Biol.* **305**, 891-904.
25. Albers, S.-V., Konings, W. N. & Driessen, A. J. M. (1999). A unique short signal sequence in membrane-anchored proteins of Archaca. *Mol. Microbiol.* **31**, 1595-1596.

26. Quiocho, F. A., Gilliland, G. L. & Phillips, G. N. (1977). The 2.8-Å resolution structure of the L-arabinose-binding protein from *Escherichia coli*. Polypeptide chain folding, domain similarity, and probable location of sugar-binding site. *J. Biol. Chem.* **252**, 5142-5149.
27. Newcomer, M. E., Gilliland, G. L. & Quiocho, F. A. (1981). L-Arabinose-binding protein-sugar complex at 2.4 Å resolution. Stereochemistry and evidence for a structural change. *J. Biol. Chem.* **256**, 13213-13217.
28. Mowbray, S. L. & Petsko, G. A. (1983). The X-ray structure of the periplasmic galactose binding protein from *Salmonella typhimurium* at 3.0-Å resolution. *J. Biol. Chem.* **258**, 7991-7997.
29. Mowbray, S. L. & Cole, L. B. (1992). 1.7 Å X-ray structure of the periplasmic ribose receptor from *Escherichia coli*. *J. Mol. Biol.* **225**, 155-175.
30. Dutzler, R., Wang, Y.-F., Rizkallah, P. J., Rosenbusch, J. P. & Schirmer, T. (1996). Crystal structures of various maltooligosaccharides bound to maltoporin reveal a specific sugar translocation pathway. *Structure,* **4**, 127-134.
31. Chaudhuri, B. N., Ko, J., Park, C., Jones, T. A. & Mowbray, S. L. (1999). Structure of D-allose binding protein from *Escherichia coli* bound to D-allose at 1.8 Å resolution. *J. Mol. Biol.* **286**, 1519-1531.
32. Auerbach, G., Huber, R., Graettinger, M., Zaiss, K., Schurig, R., Jaenicke, R. & Jacob, U. (1997). Closed structure of PGK from *Thermotoga maritima* reveals the catalytic mechanism and determinants of thermal stability. *Structure,* **5**, 1475-1483.
33. Auerbach, G., Jacob, U., Graettinger, M., Zaiss, K., Schurig, R. & Jaenicke, R. (1997). PGK from *Thermotoga maritima*. *Biol. Chem.* **378**, 327-329.
34. Auerbach, G., Ostendorp, R., Prade, L., Korndoerfer, I., Dams, T., Huber, R. & Jaenicke, R. (1998). LDH from the hyperthermophilic bacterium *Thermotoga maritima* reveals the catalytic mechanism and determinants of thermal stability. *Structure,* **6**, 769-781.
35. Maes, D., Zeelen, J. P., Thanki, N., Beaucamp, N., Alvarez, M., Thi, M. H. D., Backmann, J., Martial, J. A., Wyns, L., Jaenicke, R. & Wierenga, R. K. (1999). The crystal structure of triosephosphate isomerase (TIM) from *Thermotoga maritima*: a comparative thermostability structural analysis of ten different TIM structures. *Proteins: Struct. Funct. Genet.* **37**, 441-453.
36. Szilágyi, A. & Závodsky, P. (2000). Structural differences between mesophilic, moderately thermophilic and extremely thermophilic protein subunits: results of a comprehensive survey. *Structure,* **8**, 493-504.
37. Yip, K. S. P., Stillman, T. J., Britton, K. L., Artymiuk, P. J., Baker, P. J., Sedelnikova, S. E., Engel, P. C., Pasquo, A., Chiaraluce, R. & Cosalvi, V. (1995). The structure of *Pyrococcus furiosus* GluDH reveals a key role for ionpair networks in maintaining enzyme stability at extreme temperatures. *Structure,* **3**, 1147-1158.
38. Macedo-Ribeiro, S., Darimont, B., Sterner, R. & Huber, R. (1996). Small structural changes account for the high thermostability, of 1[4Fe-4S] ferrdoxin from *Thermotoga maritima*. *Structure,* **4**, 1291-1301.
39. Jaenicke, R. & Boehm, G. (1998). The stability of proteins in extreme environments. *Curr. Opin. Struct. Biol.* **8**, 738-748.
40. Matthews, B. W. (1996). Structural and genetic analysis of the folding and function of T4 lysozyme. *FASEB J.* **10**, 35-41.
41. Colacino, F. & Crichton, R. R. (1997). Enzyme thermostabilization: the state of the art. *Biotechnol. Genet. Eng. Rev.* **14**, 211-277.
42. Greller, G., Horlacher, R., DiRuggiero, J. & Boos, W. (1999). Molecular and biochemical analysis of MalK, the ATP-hydrolyzing subunit of the trehalose maltose transport system of the hyperthermophilic archaeon *Thermococcus litoralis*. *J. Biol. Chem.* **274**, 20259-20264.
43. Boos, W. & Shuman, H. A. (1998). The maltose/maltodextrin system of *Escherichia coli*; transport, metabolism and regulation. *Microbiol. Mol. Biol. Rev.* **62**, 204-229.
44. Baneyx, F. & Georgiou, G. (1991). Construction and characterization of *Escherichia coli* strains deficient in multiple secreted proteases: protease III degrades high-molecular-weight substrates *in vivo*. *J. Bacteriol.* **173**, 2696-2703.
45. Kabsch, W. (1993). Automatic processing of rotation diffraction data from crystals of initially unknown symmetry and cell constants. *J. Appl. Crysallog.* **26**, 795-800.
46. Otwinowski, Z. & Minor, W. (1996). Processing of X-ray diffraction data collected in oscillation mode. *Methods Enzymol.* **276**, 307-326.
47. Collaborative Computational Project Number 4 (1994). The CCP4 suite: programs for protein crystallography. *Acta Crystallog. sect. D,* **50**, 760-763.
48. Terwilliger, T. C. & Berendzen, J. (1999). Automated structure solution for MIR and MAD. *Acta Crystallog. sect. D,* **55**, 849-861.
49. De La Fortrelle, & Bricogne, G. (1997). Maximum-likelihood heavy-atom parameter refinement for multiple isomorphous replacement and multiwavelength anomalous diffraction methods. *Methods Enzymol.* **276**, 472-494.
50. Abrahams, J. P. & Leslie, A. G. W. (1996). Methods used in the structure determination of F_1-ATPase. *Acta Crystallog. sect. D,* **52**, 30-42.
51. Diederichs, K. (2000). Computing in macromolecular crystallography using a parallel architecture. *J. Appl. Crystallog.* **33**, 1154-1161.
52. Kleywegt, G. J. & Jones, T. A. (1997). Taking the fun out of map interpretation. *CCP4-ESF-EACBM Newsletter Protein Crystallog.* **33**, 19-21.
53. Bruenger, A. T., Adams, P. A., Clore, G. M., DeLano, W. L., Gros, P., Grosse-Kunstleve, R. W., Jiang, J.-S., Kuszewski, J., Nilges, M., Parma, N. S., Read, R. J., Rice, L. M., Simonson, T. & Warren, G. L. (1998). Crystallography and NMR system: a new software suite for macromolecular structure determination. *Acta Crystallog. sect. D,* **54**, 905-921.
54. Jones, T. A., Zou, J.-Y., Cowan, S. W. & Kjeldgaard, M. (1991). Improved methods for building protein models in electron density maps and the location of errors in these models. *Acta Crystallog. sect. A,* **47**, 110-119.
55. Lamzin, V. S. & Wilson, K. S. (1993). Automated refinement of protein models. *Acta Crystallog. sect. D,* **49**, 129-149.
56. Laskowski, R. A., MacArthur, M. W., Moss, D. S. & Thornton, J. M. (1993). PROCHECK: a program to check the stereochemical quality of protein structures. *J. Appl. Crystallog.* **26**, 283-291.
57. Vriend, G. (1990). WHAT IF: a molecular modeling and drug design program. *J. Mol. Graph.* **8**, 52-56.
58. Kabsch, W. & Sander, C. (1983). Dictionary of protein secondary structure: pattern recognition of

hydrogen bond and geometrical features. *Biopolymers,* **22**, 2577-2637.
59. Jean-Charles, A., Nicholls, A., Sharp, K., Honig, B., Tempczyk, A., Hendrickson, T. F. & Still, W. C. (1991). Electrostatic contributions to solvation energies: comparisons of free energy perturbation and continuum calculations. *J. Am. Chem. Soc.* **113**, 1454-1455.

Edited by T. Richmond

(Received 29 June 2000; received in revised form 8 November 2000; accepted 15 November 2000)